Lab on a Chip

PAPER

View Article Online
View Journal

Cite this: DOI: 10.1039/d6lc00265j

A dual-mode vertical flow assay for species-specific identification and total bacteria load assessment from a single urine sample

Shu-Yun Sheu,[a] Ching-Fen Shen*[b] and Chao-Min Cheng *[a]

Received 26th March 2026,
Accepted 25th May 2026

DOI: 10.1039/d6lc00265j

rsc.li/loc

Rapid urine screening would benefit from simultaneous determination of pathogen identity and clinically relevant bacteria burden, yet most paper-based assays provide only one of these outputs. Here, we report a dual-mode vertical flow assay that combines species-specific HRP-antibody/TMB immunodetection with WST-8–mPMS metabolic quantification in spatially separated detection spots within an integrated vertical flow assay device. The device employs a vertically layered membrane stack with graded pore sizes to regulate capillary-driven flow and residence time, enabling efficient analyte transport and signal development. Quantitative analysis is achieved using smartphone-based RGB imaging converted to grayscale intensity. This platform enables simultaneous bacteria identification and quantification from a single urine sample, demonstrating threshold-oriented detection around the clinically relevant bacteriuria level of 10^5 CFU mL^{-1} in both tryptic soy broth and urine samples. This work demonstrates a dual-mode vertical flow assay capable of simultaneously identifying bacteria species and estimating bacteria burden, providing a practical strategy for rapid threshold-oriented urine screening at the point-of-care.

Introduction

VFAs are an emerging class of paper-based diagnostic platforms that direct samples vertically through stacked porous layers, where capillary forces and controlled pore gradients regulate fluid transport and reaction kinetics.[1–6] Compared with LFAs, the architecture of VFAs provides faster flow rates, more uniform reagent–sample interactions, and higher compatibility with multiplexed layouts, while maintaining a simple, low-cost workflow suitable for POCT.[2,7–14] This vertical configuration minimizes nonspecific carryover, stabilizes baseline signals, and promotes consistent colorimetric development that can be readily quantified using smartphones or portable readers, while also enabling multiplexed detection of multiple targets with high specificity.[2–5,10–13,15–17]

These characteristics make VFAs particularly attractive for infection screening, where rapid and quantitative results are required without the need for laboratory instruments.[3,6,16] For example, in urine-based bacteria diagnostics, *E. coli* is the predominant causative agent of UTIs, accounting for approximately 75–85% of uncomplicated UTI cases, making it a clinically relevant primary target for species-specific detection.[18,19] Conventional culture remains the gold standard but is too time-consuming, while molecular and immunoassay-based methods require specialized equipment and trained personnel.[1,2,11,15,20–24] LFAs, although widely used in POCT, generally provide only qualitative results and are prone to background interference in complex matrices such as urine and whole blood.[2,10,15,16,21,25] VFAs overcome these limitations by combining rapid capillary-driven flow with tunable residence time and enhanced analyte retention, providing a versatile and quantitative paper-based alternative for on-site microbial detection.[3,6,16,26]

Recent research on VFAs includes work in immunoassays, nucleic-acid detection, protein biomarkers, whole-blood testing, and AI-augmented optical readouts, collectively underscoring the versatility of the vertical format. In the field of pathogen detection, Kaur and Eltzov reported an HRP-antibody/TMB scheme augmented with a polyvinyl alcohol time barrier and lactose stabilization to improve the stability of antigen–antibody binding and extend reagent shelf-life, markedly lowering the LOD.[16] In the field of nucleic acids, Tahmasebi *et al.* amplified the hepatitis B virus X gene by PCR and generated HRP chemiluminescence on a VFA, achieving sensitivity comparable to that of clinical real-time PCR with a simpler workflow.[20] Regarding protein biomarkers, Wang *et al.* developed gold-nanoparticle-conjugated antibodies and built a smartphone-quantified VFA platform for acute

[a] *Institute of Biomedical Engineering, National Tsing Hua University, Hsinchu 300, Taiwan. E-mail: chaomin@mx.nthu.edu.tw*
[b] *Department of Pediatrics, National Cheng Kung University Hospital, College of Medicine, National Cheng Kung University, Tainan 701, Taiwan. E-mail: drshen1112@gmail.com*

kidney injury markers (neutrophil gelatinase-associated lipocalin, cystatin C, retinol-binding protein 4), achieving ~1 ng mL^{-1} (single-analyte) and 5 ng mL^{-1} (multi-analyte) performance, demonstrating the advantages of vertical-flow multiplex detection.[12] In another study, Lei *et al.* quantified interleukin-6 in serum within 15–20 min using optimized 0.2 μm pore size membranes and multiple control zones examined *via* image analysis to ensure accuracy, achieving an LOD of 3.2 pg mL^{-1} in serum.[11] With respect to whole-blood compatibility, Serhan *et al.* separated plasma within a multilayer stack by leveraging pore-size differences, and measured total iron from finger-prick blood in ~5 min via colorimetry, thus eliminating centrifugation.[25]

In addition to the abovementioned advances, progress in optical and data-science continues to enhance analytical sensitivity. Goncharov *et al.* introduced a paper-based fluorescent VFA for three cardiac injury markers (myoglobin, creatine kinase–muscle/brain type, heart-type fatty acid-binding protein), using deep learning to normalize spatial signals, which yielded strong correlation with ELISA and achieved LODs below 0.52 ng mL^{-1} for all three biomarkers.[15] In another example of advanced optical integration, Chen *et al.* employed magnetic surface-enhanced raman scattering nanotags (Fe_3O_4@Au core–shell) for ultrasensitive multiplex detection of mycotoxins in complex food matrices, achieving signal enhancements of approximately three orders of magnitude compared with conventional gold-nanoparticle assays.[27] Despite these advances, few VFAs are capable of providing both species identification and total bacteria load from urine within a single, low-complexity workflow explicitly aligned to a clinical threshold.

To address the growing demand for accessible, rapid, and specific detection of bacteria pathogens, we developed a VFA platform featuring multiple engineering innovations for simultaneous species-specific identification and quantitative POCT. The integrated device contains four spatially separated detection spots within the same VFA device: two spots for HRP-antibody/TMB-based species-specific immunodetection and two spots for WST-8–mPMS-based metabolic quantification, enabling parallel readouts from a single urine

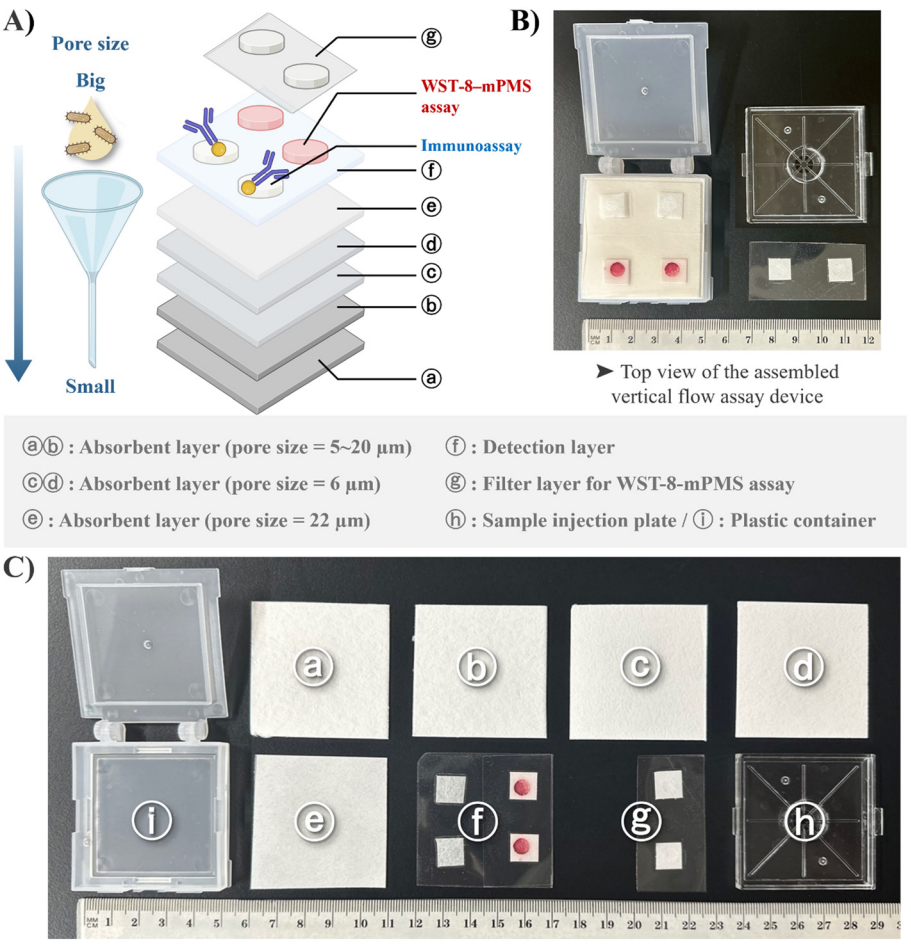

Fig. 1 Design and structure of the integrated dual-mode VFA device. (A) Schematic illustration of the integrated VFA device with spatially separated detection spots for the WST-8–mPMS metabolic assay and HRP-antibody/TMB immunoassay. The graded-pore paper stack guides vertical capillary flow through the device. (B) Top view of the assembled VFA device, including the plastic container, sample injection plate, and detection layers. (C) Exploded view of the device components, including absorbent layers, detection layer, filter layer, sample injection plate, and plastic container.

sample while minimizing chemical and optical interference between the two colorimetric reactions (Fig. 1A). First, we employed a simplified immunoassay using a single primary antibody directly conjugated with HRP, eliminating secondary antibodies to reduce steps, cost, and time (Fig. 2). This one-step detection approach offers a more practical and efficient solution for use in resource-limited settings. Second, the detection layer in our device used PT-R7 paper-based material, a high-capillarity conjugate-release matrix with interwoven cellulose–glass fibers that supports high loading, passive protein adsorption, uniform rehydration, and dry-storage stability.[24,28–34] This material facilitates uniform fluid penetration, prolongs antigen–antibody interaction time, and enables efficient protein immobilization with controlled release after rehydration.[24,28,30–32] Third, we integrated smartphone-based RGB colorimetry under standardized lighting, converting RGB values to grayscale intensities for quantitative evaluation without benchtop readers (Fig. 2). This approach enables instrument-free quantitative interpretation compatible with digital health workflows, supporting seamless integration with mobile-based data analysis and remote clinical decision-making, thereby enhancing the practicality of the platform for POCT and decentralized testing. Fourth, a funnel-like absorbent stack with a graded pore structure was placed beneath the detection plane to tune residence time, concentrate analytes at the reaction interface, and suppress downward diffusion of immunocomplexes. This configuration also facilitated the removal of unbound antibodies, thereby improving signal clarity and sensitivity (Fig. 1A–C).

For total bacteria load assessment, the WST-8–mPMS metabolic readout was adapted from a viable microorganism detection strategy previously developed by our group.[35] In this system, WST-8 serves as a tetrazolium salt that is reduced to a water-soluble formazan product, while mPMS functions as an intermediate electron mediator. EDTA is used to transiently increase bacteria cell wall permeability,

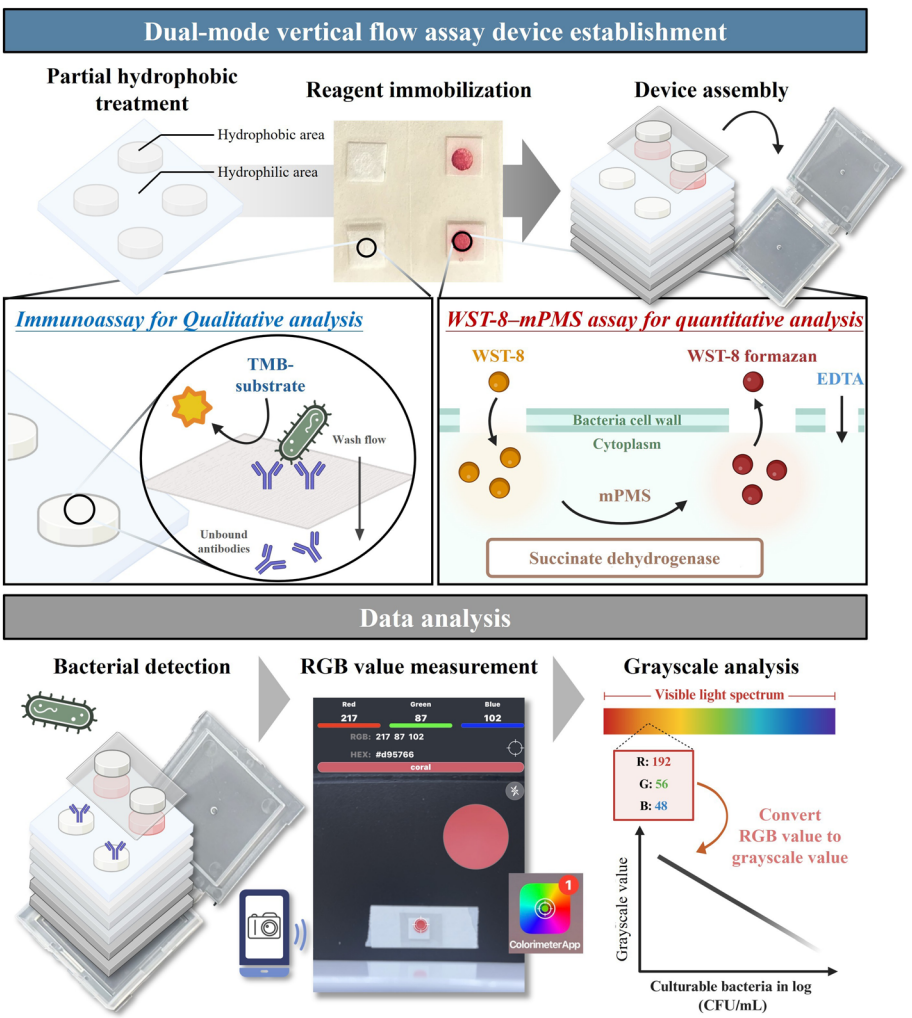

Fig. 2 Workflow and detection principles of the dual-mode VFA. The device fabrication process includes partial hydrophobicity treatment, reagent immobilization, and device assembly. The platform contains two spatially separated detection modules: an HRP-antibody/TMB immunoassay for species-specific qualitative identification and a WST-8–mPMS metabolic assay for quantitative total bacteria load assessment. After sample loading, colorimetric signals are recorded by smartphone imaging, extracted as RGB values, and converted to grayscale intensity for data analysis. The figure was created using https://BioRender.com.

allowing the reagent system to couple with intracellular metabolic activity. In metabolically active bacteria, endogenous dehydrogenase activity transfers electrons through mPMS to WST-8, resulting in formazan formation. Therefore, the colorimetric signal reflects viable bacterial metabolic activity and provides a species-independent readout of total bacteria load (Fig. 2). Finally, the HRP-antibody/TMB immunodetection module and the WST-8–mPMS metabolic module enable simultaneous species-specific identification and total bacteria load assessment from a single urine sample within one integrated VFA device (Fig. 1A–C and 2).

The combination of layered material engineering, simplified immunochemistry, mobile quantification, and device-level integration provides a novel and versatile platform with strong potential for practical use in clinical and environmental microbiological diagnostics. To evaluate its analytical performance, the assay was tested across bacteria concentrations centered around 10^5 CFU mL^{-1}, corresponding to the clinically significant bacteriuria threshold commonly used for urinary tract infection screening.[22–24] Here, 10^5 CFU mL^{-1} was used as a clinically relevant decision threshold for assay evaluation rather than as a formally calculated limit of detection. This approach ensured that device performance directly reflected screening and triage decision levels. We further demonstrated species-specific immunoassay detection in both TSB and urine, quantitative trends for total bacteria load across multiple species and matrices, and integrated a cartridge operation that enabled simultaneous metabolic and immunological readouts from a single sample. Rather than maximizing analytical sensitivity, this work introduces a clinically aligned sensing paradigm that simultaneously resolves pathogen identity and decision-level bacteria burden within a single assay.

Experimental section

Reagents and materials

E. coli DH5α (BCRC No. 51731) and *S. aureus* subsp. aureus (BCRC No. 12989) were obtained from the Bioresource Collection and Research Center (BCRC, Hsinchu, Taiwan). Paper-based substrates used for device fabrication and flow optimization included Whatman filter papers (Lot No. 1002-150, 1003-185, 1004-240, 1005-185, 1006-185, 1440-150/185, 1441-185, 1442-185, 1454-185, and 1542-185; Cytiva Life Sciences, Marlborough, MA, USA), ADVANTEC filter papers (Lot No. 5A, 5B, and 5C; Toyo Roshi Kaisha, Ltd., Tokyo, Japan), PT-R7 conjugate-release membranes (Model R-1343/1554, Lot No. 343438F; MDI Technologies, Ambala, Haryana, India), and blotting papers (Model FP-1, Catalog No. OWFP1, 20 × 20 cm, 100 sheets per box; Thermo Fisher Scientific, Waltham, MA, USA). The plastic container and sample injection plate were adapted from the Watson Co., Ltd. Plasma Separation Device (Cat. No. 176-600C, Tokyo, Japan).

HRP conjugation Kit, Lightning-Link® (ab102890), 3,3′,5,5′-tetramethylbenzidine (TMB) substrate solution (ab99995), and anti-*E. coli* LPS monoclonal antibody (ab35654, 100 μg) were purchased from Abcam (Cambridge, UK). Bovine serum albumin (BSA, ≥98%, Cat. No. A7906, CAS 9048-46-8), tryptic soy broth (TSB, NutriSelect® Basic, Cat. No. T8907-500G), and phosphate-buffered saline (PBS, Cat. No. P4417-50TAB) were obtained from Sigma-Aldrich (St. Louis, MO, USA). Tween 20 (Cat. No. TB0560, CAS 9005-64-5) was supplied by Bio Basic Inc. (Markham, ON, Canada). Ethylenediaminetetraacetic acid (EDTA, MW 292.25, CAS 60-00-4, Cat. No. 8991-01) was obtained from J. T. Baker (Phillipsburg, NJ, USA). WST-8 (2-[2-methoxy-4-nitrophenyl]-3-[4-nitrophenyl]-5-[2,4-disulfophenyl]-2*H*-tetrazolium sodium salt) and mPMS (1-methoxy-5-methylphenazinium methyl sulfate) were purchased from IMT Formosa New Materials Co., Ltd. (Kaohsiung, Taiwan).

Water-soluble red ink (LIFE No. 100, red, 10 mL, water-based refill ink for automatic stamps) was purchased from a local stationery store (Hsinchu, Taiwan). Scanning electron microscopy (SEM) images were obtained using a JEOL IT800 field-emission scanning electron microscope. Colorimetric signal analysis was performed using the Colorimeter App (iOS; free download: https://apps.apple.com/ee/app/colorimeter-app/id1542365656). Deionized water (18.2 MΩ·cm, ddH_2O) was used in all experiments, and all reagents were of analytical grade unless otherwise stated.

Water-soluble red ink flow test

To identify an optimal paper-based material combination that ensures stable, rapid, and uniform fluid flow within the detection device, red ink was used as a preliminary fluid model to visualize capillary flow behavior and optimize layer configurations. Because the vertical flow system is primarily governed by capillary-driven liquid transport rather than particle-specific interactions, the dye solution provides a convenient approximation for evaluating flow distribution and residence time during device optimization.

The evaluated parameters included thickness (μm), pore size (μm), and wet burst strength (psi) (Table S1). Based on pore size and experimental requirements, all paper substrates were classified into three groups: group 1 (samples ①–③), group 2 (samples ④–⑥ and ⑪), and group 3 (samples ⑦–⑩, ⑫, and ⑬). To assess the applicability of these materials in vertical flow detection devices, we conducted a series of water-soluble red ink flow tests designed to evaluate flow uniformity and stability. Water-soluble red ink was chosen because its high visibility allowed direct visualization of capillary transport through multilayer paper structures. The paper substrates were primarily sourced from two manufacturers: Whatman (samples ①–⑩) and ADVANTEC (samples ⑪–⑬). Their specific models and physical properties were extracted from the manufacturers' official databases (Whatman: https://www.cytivalifesciences.com/en/us; ADVANTEC: https://www.advantec.co.jp/en/). These data served

as the initial criteria for material selection in subsequent experiments aimed at optimizing device fabrication and performance.

For flow testing, Whatman substrates were first assembled in layered stacks according to the experimental design, with a blotting paper sheet placed at the bottom as the absorbent layer to capture excess fluid after applying 1 mL of water-soluble red ink. The stacking arrangements are detailed in Table S2. The flow behavior of the top layer was directly observed, while flow through the second and third layers was quantified using a timing method, recording the elapsed time until the ink reached the bottom blotting paper. These measurements enabled evaluation of both flow uniformity and transport efficiency. Subsequently, untested ADVANTEC substrates were integrated with the Whatman substrates to generate 11 new stacked combinations, organized by pore size, as shown in Table S3. Each combination was tested under identical conditions, with flow time, uniformity, and stability recorded as key metrics. The results of these experiments provided the basis for selecting the most suitable paper-based material combinations to support the development and optimization of the VFA device, as summarized in Tables S4 and S5.

Scanning electron microscopy

Scanning electron microscopy imaging was performed to verify bacterial transport and retention within the optimized paper-based vertical flow structure. Based on the optimized parameters obtained from the red ink assay, a layered configuration consisting of Whatman 1454–185 as the first layer and Whatman 1003-185 as the second layer was selected. *S. aureus* (10^8 CFU mL^{-1}) was applied onto the stacked substrates, while ddH_2O was used as the control. Bacteria penetration and retention in the lower layers were examined by SEM. Prior to imaging, samples were sputter-coated with an approximately 3 nm platinum layer to enhance conductivity. SEM analysis was performed at an accelerating voltage of 5 kV under high-vacuum conditions, and images were acquired at 10 000× and 20 000× magnifications to visualize bacteria cells and paper microstructures.

Device configuration and fabrication

The optimized paper substrates and PT-R7 membrane were cut into 1 cm × 1 cm squares using a paper cutter. To guide sample delivery toward predefined reaction zones, circular openings (0.6 cm in diameter) were created in laminating films using a hole puncher. These films were aligned with paper substrates and processed under heat-lamination conditions, yielding detection layers with guided hydrophilic reaction zones rather than fully enclosed microfluidic channels.

For the integrated dual-mode VFA, four independent detection spots were arranged within the same plastic container. Two spots were assigned to the HRP-antibody/TMB-based species-specific immunodetection module, while the other two spots were assigned to the WST-8–mPMS-based metabolic quantification module. These detection spots were spatially separated to minimize chemical and optical interference between the two colorimetric reactions while enabling parallel readouts from a single urine sample within one device. The sample injection plate contained guided flow channels to direct the sample and washing buffer into the predefined detection spots in a stable and controlled flow direction (Fig. 1A–C).

For the HRP-antibody/TMB immunodetection module, the vertical flow device was constructed with a layered configuration composed of a detection layer and a multi-layer absorbent layer. The detection layer consisted of a PT-R7 membrane patterned with hydrophilic channels to define the immunodetection spots for antigen recognition and signal generation. The absorbent layer was assembled as a five-layer structure arranged sequentially from top to bottom: one sheet of Whatman No. 1454 (pore size ≈ 22 μm), two sheets of Whatman No. 1003 (pore size ≈ 6 μm), and two sheets of blotting paper with high absorbency. This vertical pore gradient guided fluid transport through the stack. The assembled substrates were placed into a plastic container, with a sample injection plate mounted above the detection layer to facilitate sample loading. The overall configuration is shown in Fig. 1B and C. This configuration provided a controlled capillary pressure gradient, enabling reproducible downward flow and enhanced residence time at the detection interface.

For the WST-8–mPMS metabolic quantification module, a simplified two-layer format was used during module-level optimization and standalone performance evaluation, consisting of a filtration layer (Whatman 1454-185) on the top and a detection layer (Whatman 1003-185) on the bottom. The same WST-8–mPMS-based metabolic detection principle was then incorporated into the integrated dual-mode device as spatially separated metabolic detection spots. To improve handling and stability, the detection layer was supported by a transparent laminating film at its base, serving as a backing layer.

HRP-antibody conjugation

HRP-antibody conjugation was performed using an HRP conjugation kit. Prior to use, all reagents and consumables were equilibrated to room temperature (20–25 °C). Antibodies were purified and dissolved in PBS (pH 7.2–7.4). Buffers containing primary amines (*e.g.*, glycine, ethanolamine) or thiol compounds (*e.g.*, dithiothreitol, β-mercaptoethanol) were strictly avoided, as these interfere with the conjugation reaction.

For the conjugation reaction, 1 μL of modifier reagent was added per 10 μL of antibody solution, followed by gentle mixing to ensure homogeneity. The HRP conjugation mix vial was then opened, and the antibody–modifier mixture was pipetted directly onto the thawed HRP mix. The solution was gently mixed by pipetting up and down 1–2 times to ensure

complete dissolution. The conjugation mixture was incubated at 25 °C for 3 h in the dark. Following incubation, 1 μL of quencher reagent was added per 10 μL of reaction mixture. The solution was gently mixed and allowed to stand for 30 min at room temperature to terminate the reaction and stabilize the conjugates. The resulting HRP-antibody conjugates required no further purification and were stored at 4 °C for up to 18 months. For long-term storage, conjugates were supplemented with 50% glycerol and stored at −20 °C in the dark. Repeated freeze–thaw cycles were avoided to preserve antibody activity. Successful conjugation was verified by visible color change and confirmed by comparing HRP activity between conjugated and unconjugated controls.

Antibody immobilization and blocking

The HRP-conjugated primary antibody was diluted 1 : 500 in PBS and subsequently mixed at a 1 : 1 (v/v) ratio with blocking buffer (PBS supplemented with 0.05% Tween 20 and 1% BSA). A 20 μL aliquot of the antibody–blocking buffer mixture was then dispensed onto the hydrophilic center of the detection layer corresponding to the HRP-antibody/TMB immunodetection spots. To ensure efficient adsorption and prevent enzyme inactivation, all procedures were performed within a biosafety cabinet, and the samples were incubated in the dark for 2 h. This treatment promoted stable antibody immobilization while minimizing nonspecific binding through BSA blocking, thereby supporting the sensitivity and specificity of subsequent immunoassays.

Sample loading and washing

To evaluate device sensitivity across different bacteria concentrations, *E. coli* suspensions were serially diluted in TSB and human urine to final concentrations of 10^8, 10^7, 10^6, 10^5, and 5×10^4 CFU mL^{-1}. For each assay, the prepared sample was applied onto the top of the device through the sample injection plate, which guided liquid delivery toward the predefined detection spots. The sample then infiltrated naturally into the detection layer by capillary action, ensuring complete contact with the reaction zones for antigen–antibody binding. The devices were incubated at room temperature (22–25 °C) for 30 min without agitation to maintain consistency across tests. Following incubation, unbound antibodies and residual interfering substances were removed by a washing step. This washing step was required for the HRP-antibody/TMB immunodetection module to reduce background signals and improve species-specific signal clarity. The PBS containing 0.05% Tween 20 was dispensed dropwise onto the top of the device through the guided sample injection plate, enabling flow through the paper matrix *via* capillary action. The washing procedure was repeated twice to ensure thorough cleaning of the reaction zone and to reduce background signals. Care was taken to avoid rapid dispensing, which could disturb antigen–antibody complexes bound within the detection layer. Because liquid transport was guided by the sample injection plate and driven by the absorbent paper stack, no active pumping or external fluidic equipment was required.

Colorimetric reaction

Following the washing step, the detection layer was placed on a white background. A 10 μL aliquot of TMB substrate solution was directly added to the reaction zone. TMB color development began immediately after substrate addition, and images were acquired at a standardized endpoint of approximately 3 min to ensure consistent readout timing across all samples. The oxidized TMB product was observed as a blue coloration, reflecting HRP enzymatic activity and indicating antigen–antibody binding.

Image acquisition and data analysis

For both the HRP-antibody/TMB immunodetection module and the WST-8–mPMS metabolic module, colorimetric signals were quantified by smartphone-based RGB extraction, white-reference normalization, and grayscale conversion. After the colorimetric reaction, images of the detection zones were immediately captured using a smartphone. To ensure consistency, all images were taken under identical lighting and exposure settings to minimize variability across tests. A white reference background was used for normalization across images. Image analysis was performed using the Colorimeter App (iOS, free download: https://apps.apple.com/ee/app/colorimeter-app/id1542365656), which extracts real-time intensity values of red, green, and blue channels (Fig. 2).

For each reaction zone, RGB values were obtained by averaging a fixed circular ROI centered within the reaction spot to minimize edge effects and spatial heterogeneity. The same ROI size and placement rule were applied across all samples. To reduce the influence of illumination variation, camera settings, and strip-to-strip background differences, a white reference region on the same test strip/device was used as an internal reference for RGB normalization before grayscale conversion. Each RGB channel of the reaction zone was normalized against the corresponding white reference value according to $R' = R/(R_{white}/255)$, $G' = G/(G_{white}/255)$, and $B' = B/(B_{white}/255)$. The normalized RGB values were then converted into a single grayscale intensity using a weighted luminance formula: Grayscale = $0.229 \times R' + 0.587 \times G' + 0.114 \times B'$, reflecting the relative contributions of red, green, and blue channels to perceived brightness. This device-specific white-reference normalization was applied once for each device and was used to reduce variations caused by lighting conditions, smartphone imaging, and differences in background brightness among test strips. Normalized grayscale intensity was calculated as the difference between the background/reference region and the detection zone signals. This normalization strategy compensates for intrinsic sample coloration, including the yellowish background commonly observed in urine, by referencing each reaction zone to its local background.

Calibration curves were then generated by nonlinear regression using the Hill equation:

$$Y = (B_{max}X^h)/(K_d^h + X^h)$$

where Y is the normalized grayscale, X is the bacteria concentration, B_{max} is the maximum response, K_d is the apparent dissociation constant, and h is the Hill coefficient. This model provided robust fitting of the nonlinear dose–response relationship and enabled back-calculation of bacteria concentrations in unknown samples.

Total bacteria quantification (WST-8–mPMS assay)

An appropriate amount of WST-8 (2-[2-methoxy-4-nitrophenyl]-3-[4-nitrophenyl]-5-[2,4-disulfophenyl]-2*H*-tetrazolium, molecular weight 600.48) was weighed and dissolved in ddH_2O to prepare solutions of various concentrations. Similarly, mPMS powder was weighed and dissolved in ddH_2O at different concentrations. Additionally, EDTA was dissolved in ddH_2O to prepare a 10^{-5} M solution. EDTA was included to transiently permeabilize bacteria cell walls, thereby enhancing the coupling between intracellular dehydrogenase activity and WST-8 reduction.

To prepare the WST-8–mPMS detection reagent, WST-8 and mPMS solutions were mixed at a 1 : 1 volume ratio. This reagent, together with the EDTA solution, was drop-cast onto the surface of hydrophobically treated paper-based materials. The coated papers were then placed in a biosafety cabinet and air-dried overnight to ensure stable immobilization of the reagents. After complete drying, the treated paper substrates were sequentially stacked, layer by layer, according to the designed configuration to guarantee sufficient interlayer contact.

To evaluate device performance, bacteria suspensions at various concentrations were added to the top paper layer containing EDTA. The sample then passed through the filtration layer and reached the WST-8–mPMS-loaded detection layer by capillary flow. In metabolically active bacteria, endogenous dehydrogenase activity reduced WST-8 through mPMS-mediated electron transfer, producing a water-soluble orange formazan product. Color changes were monitored within 20 min after sample application to confirm the device's ability to detect total bacteria load.

Bacteria quantification and RGB value analysis

For total bacteria load detection, bacteria suspensions of *E. coli* and *S. aureus* with concentrations ranging from 10^8, 10^7, 10^6, 10^5, and 5×10^4 CFU mL^{-1} were applied to the device, and color changes in the detection layer were monitored. Quantitative analysis was performed by RGB extraction, white-reference normalization, and grayscale conversion using the same image-analysis procedure described above.

Results

Paper-based material selection by red ink flow test

To establish stable and uniform fluid flow, commercially available paper substrates from Whatman and ADVANTEC were systematically screened using a water-soluble red ink flow assay. Thirteen paper types were characterized by their physical properties, including thickness (150–390 μm), pore size (1–25 μm), and wet burst strength (0.22–7 psi) (Table S1). Based on pore size and flow behavior, these materials were grouped and vertically stacked into multi-layer configurations to evaluate their combined wicking performance (Tables S2 and S3).

Red ink flow tests revealed that combinations employing intermediate pore sizes in the upper layer (20–25 μm) coupled with smaller pores in the middle and lower layers (2–7 μm) produced the most uniform capillary-driven flow and stable transport dynamics. Among 27 initial Whatman combinations, configurations such as ③–⑥–⑧ and ③–⑥–⑦ demonstrated the shortest flow times (≈26–27 s) and superior flow uniformity, whereas assemblies composed of either overly large or overly dense papers led to uneven spreading or delayed transport (Table S4). Further optimization integrating ADVANTEC materials (samples ⑪–⑬) confirmed that graded-pore stacking enhanced fluid distribution and minimized backflow. The combination ③–⑥–⑧, featuring a moderate top-layer pore size (22 μm) and progressively decreasing porosity in the lower layers (6 μm → 2.7 μm), yielded the best compromise between flow velocity and uniform signal formation (Table S5). The final design adopted this funnel-like absorbent stack with a graded pore structure, which balanced capillary pressure and analyte retention, ensuring efficient delivery toward the reaction interface while minimizing downward diffusion of immunocomplexes. These results established a reliable paper-based architecture with reproducible vertical flow dynamics, providing a robust foundation for subsequent immunoassay integration.

Species-specific bacteria detection in TSB

Following material and structural optimization, the HRP-antibody/TMB immunoassay in a VFA was evaluated using *E. coli* suspensions prepared in TSB. A fixed volume of 1 mL was applied through the sample injection plate to guide sample delivery into the predefined immunodetection spots (Fig. 1B and C). The sample injection plate guided the liquid into the predefined immunodetection spots, and TMB-based color development produced distinct blue signals corresponding to bacteria concentration. Quantitative analysis was performed by extracting RGB values, applying white-reference normalization, and converting the normalized RGB values into grayscale intensities (Fig. 3A, B and E). The colorimetric response changed in a concentration-dependent manner across the tested *E. coli* concentration range of 5×10^4–10^8 CFU mL^{-1}, supporting threshold-oriented detection around the clinically relevant

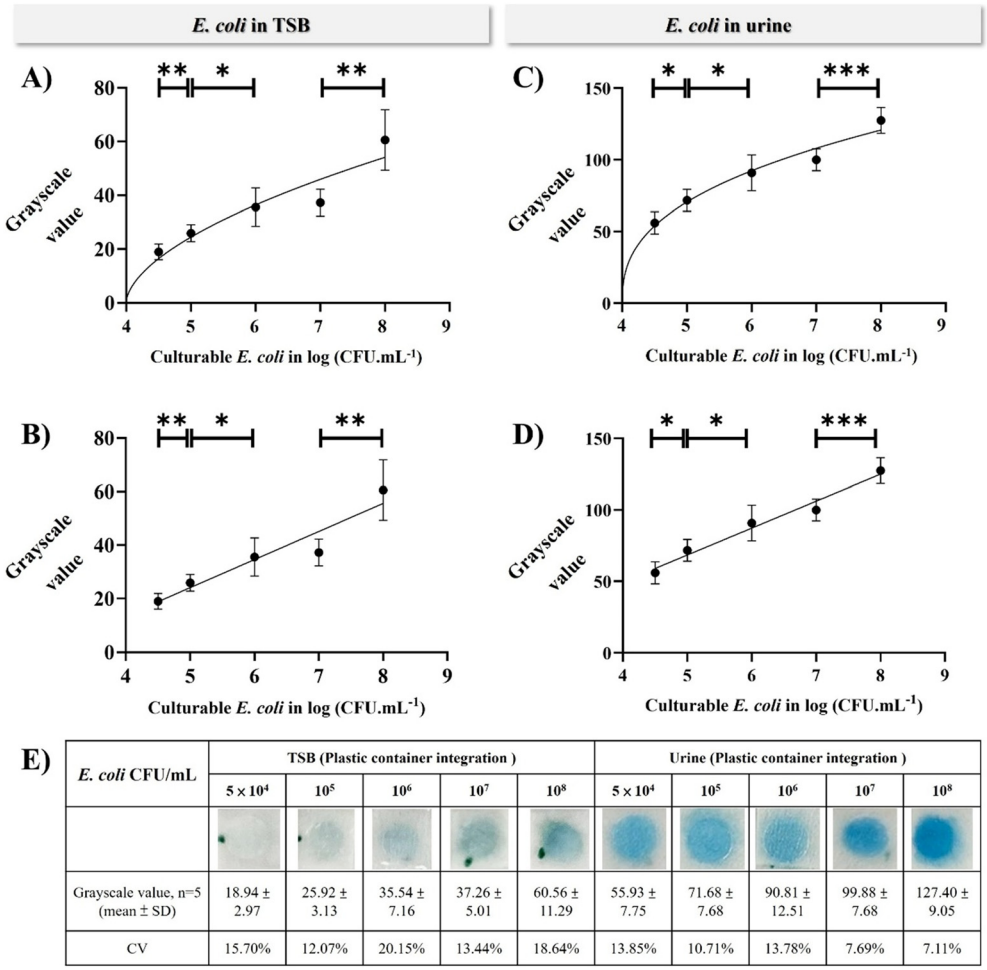

E)

E. coli CFU/mL	TSB (Plastic container integration)					Urine (Plastic container integration)				
	5×10^4	10^5	10^6	10^7	10^8	5×10^4	10^5	10^6	10^7	10^8
Grayscale value, n=5 (mean ± SD)	18.94 ± 2.97	25.92 ± 3.13	35.54 ± 7.16	37.26 ± 5.01	60.56 ± 11.29	55.93 ± 7.75	71.68 ± 7.68	90.81 ± 12.51	99.88 ± 7.68	127.40 ± 9.05
CV	15.70%	12.07%	20.15%	13.44%	18.64%	13.85%	10.71%	13.78%	7.69%	7.11%

Fig. 3 Species-specific HRP-antibody/TMB immunodetection of *E. coli* in TSB and urine using the integrated VFA device. (A and B) Calibration curves for *E. coli* detection in TSB fitted using (A) Hill and (B) linear regression models. (C and D) Calibration curves for *E. coli* detection in human urine fitted using (C) Hill and (D) linear regression models. (E) Representative colorimetric responses and grayscale quantification of *E. coli* at different concentrations in TSB and urine. Data are presented as mean ± SD (n = 5), with CV values shown for each concentration. Statistical significance is indicated as $p < 0.05$ (*), $p < 0.01$ (**), and $p < 0.001$ (***).

bacteriuria level. Hill equation fitting yielded the following model (Fig. 3A):

$$\text{Grayscale} = (84\,271 \times [E.\ coli]^{0.5730})/(K_d^{0.5730} + [E.\ coli]^{0.5730});\quad R^2 = 0.7422$$

Although model convergence of K_d was limited, a slightly stronger fit (Fig. 3B):

$$\text{Grayscale} = 10.52 \times [E.\ coli] - 28.50;\ R^2 = 0.7718$$

CV analysis revealed fluctuations at higher concentrations, with the maximum CV reaching 20.15% at 10^6 CFU mL^{-1} (Fig. 3E). The lateral color spreading observed in the reaction zones (Fig. 3E) is attributed to capillary diffusion within the porous detection matrix rather than insufficient hydrophobic confinement by lamination. Non-uniform color development, particularly at low bacteria concentrations, reflects heterogeneous enzyme distribution and capillary transport within the porous matrix; however, averaging grayscale values over a fixed region of interest mitigated local variability and enabled reliable concentration-dependent trends. These results suggest that, while the assay delivered a consistent concentration-dependent response, performance at high bacteria loads could be further stabilized. To further validate the specificity of the *E. coli* immunoassay, *S. aureus* suspensions (5×10^4–10^8 CFU mL^{-1}) were tested under the same immunoassay protocol but without integration into the plastic container system. No visible color development was observed across all concentrations (Table S6), supporting the initial specificity of the anti-*E. coli* immunoassay and minimal cross-reactivity against the tested Gram-positive non-target bacterium.

Species-specific bacteria detection in human urine

To evaluate clinical applicability, the same HRP-antibody/TMB immunodetection module was tested using untreated human

urine spiked with *E. coli* suspensions (5×10^4–10^8 CFU mL^{-1}). Distinct blue coloration and concentration-dependent contrast were maintained, demonstrating stable assay performance in complex matrices (Fig. 3C–E). Hill equation fitting yielded the following model (Fig. 3C):

$$\text{Grayscale} = (79\,127 \times [E.\ coli]^{0.3881})/(K_d^{0.3881} + [E.\ coli]^{0.3881});\quad R^2 = 0.8643$$

Although K_d convergence was limited, linear regression analysis provided an alternative fit (Fig. 3D):

$$\text{Grayscale} = 18.85 \times [E.\ coli] - 25.81;\ R^2 = 0.8764$$

CV analysis demonstrated excellent reproducibility across concentrations, with CVs of 13.85%, 10.71%, 13.78%, 7.69%, and 7.11% for 5×10^4, 10^5, 10^6, 10^7, and 10^8 CFU mL^{-1}, respectively (Fig. 3E). Despite the intrinsic coloration of urine, concentration-dependent signal trends and statistical discrimination were preserved after grayscale normalization, indicating minimal interference from sample background. Signal variation decreased at higher bacteria loads, suggesting improved saturation uniformity within the vertical flow structure. These findings indicate that the platform maintained threshold-oriented detectability in complex biological fluids, highlighting its potential applicability for UTI screening.

Total bacteria load assessment in TSB and human urine

The VFA design also allowed for implementation of alternative detection principles. In addition to immunoassay-based recognition, we developed a WST-8–mPMS metabolic VFA to quantify total bacteria load, thereby expanding the platform's applicability beyond species-specific detection. Both *E. coli* and *S. aureus* were tested using concentrations ranging from 5×10^4 to 10^8 CFU mL^{-1} in TSB and human urine. Linear regression analysis demonstrated that in TSB, *E. coli* exhibited a concentration-dependent metabolic response (Fig. 4A):

$$\text{Grayscale} = -0.1259 \times [E.\ coli] + 23.558;\ R^2 = 0.84$$

In human urine, the response remained consistent, yielding (Fig. 4B):

$$\text{Grayscale} = -4.263 \times [E.\ coli] + 195.2;\ R^2 = 0.82$$

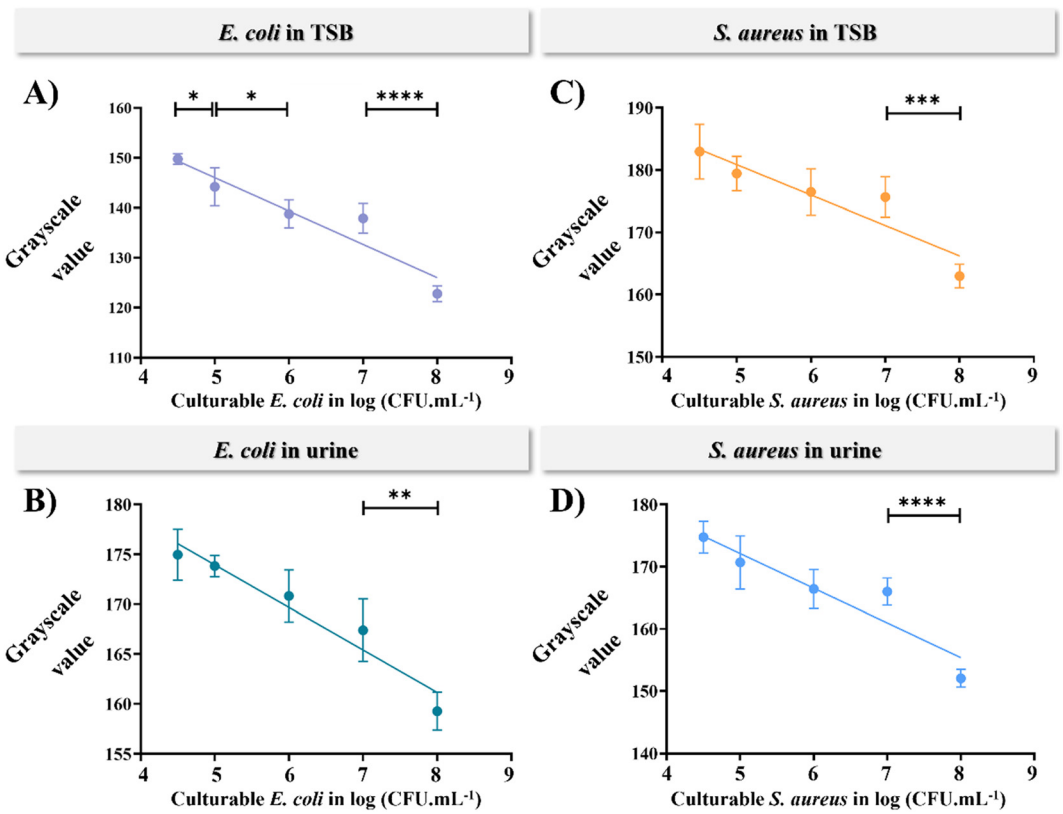

Fig. 4 WST-8–mPMS metabolic quantification of total viable bacteria load across bacteria species and sample matrices. (A and B) Quantitative detection of *E. coli* using the WST-8–mPMS metabolic assay in (A) TSB and (B) human urine. (C and D) Quantitative detection of *S. aureus* using the WST-8–mPMS metabolic assay in (C) TSB and (D) human urine. Grayscale intensity decreased with increasing bacteria concentration, reflecting stronger WST-8 reduction and formazan formation at higher viable bacteria loads. Data are presented as mean ± SD (n = 5). Statistical significance is indicated as $p < 0.05$ (*), $p < 0.01$ (**), $p < 0.001$ (***) and $p < 0.0001$ (****).

For *S. aureus*, linear fitting also supported concentration-dependent total bacteria load estimation. In TSB, the relationship was (Fig. 4C):

$$\text{Grayscale} = -4.883 \times [\textit{S. aureus}] + 205.3;\ R^2 = 0.72$$

while in human urine, the corresponding fit was (Fig. 4D):

$$\text{Grayscale} = -5.574 \times [\textit{S. aureus}] + 200.0;\ R^2 = 0.78$$

These findings demonstrate that the WST-8–mPMS metabolic VFA supports total viable bacteria load assessment across different bacteria species and sample matrices. Importantly, this demonstrates the versatility of the VFA, which can be adapted for either metabolic or immunological detection. Building upon this flexibility, we further combined the two modules into an integrated platform capable of simultaneous species-specific and quantitative bacteria detection.

Integrated species-specific and quantitative bacteria detection

To demonstrate multiplexing capability, an integrated platform combining total bacteria load assessment using the WST-8–mPMS metabolic assay and species-specific detection using the HRP-antibody/TMB immunoassay was evaluated in human urine. Each test used 1 mL of spiked *E. coli* suspension across five concentration levels (5×10^4–10^8 CFU mL^{-1}). In this integrated device, the two readouts were generated in parallel from spatially separated detection spots within the same plastic container, using the same urine sample. For total bacteria load detection, grayscale values generally increased with concentration. Statistical analysis revealed highly significant differences between 5×10^4 and 10^7 CFU mL^{-1} (***, $p < 0.001$) and between 5×10^4 and 10^8 CFU mL^{-1} (**, $p < 0.01$), indicating that the WST-8–mPMS module enabled threshold-oriented total bacteria load assessment across a concentration range spanning the clinically relevant bacteriuria level of 10^5 CFU mL^{-1} (Fig. 5A). For species-specific detection, concentration-dependent signals were observed despite variability. A statistically significant difference between 5×10^4 and 10^8 CFU mL^{-1} (***, $p < 0.001$), demonstrated that the antibody-based immunoassay module could distinguish high bacteria load from low-level bacteria concentrations within the integrated device (Fig. 5B).

Overall performance

Across all tested configurations, the VFA consistently demonstrated its ability to provide both qualitative and quantitative bacteria detection under simple operating conditions. The HRP-antibody/TMB immunoassay module enabled species-specific recognition of *E. coli* with clear visual signal discrimination in both TSB and urine. The WST-8–mPMS metabolic module further supported

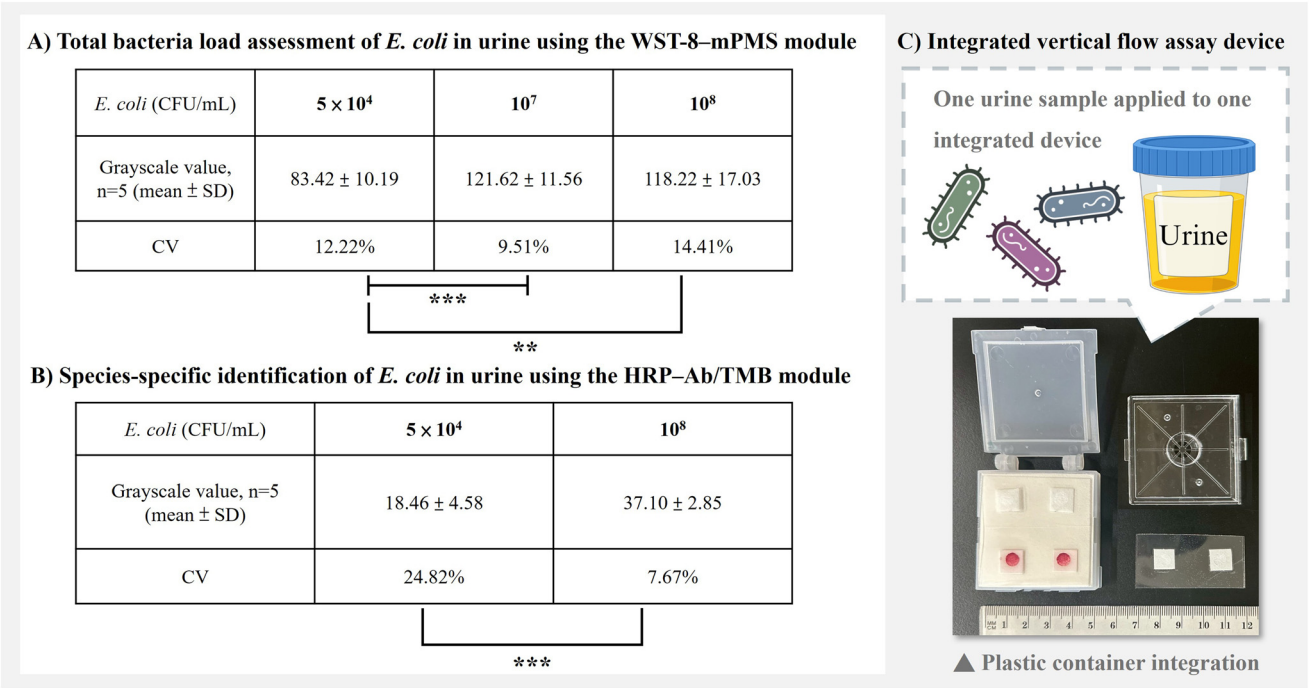

Fig. 5 Integrated dual-mode detection of *E. coli* in urine using a single VFA device. (A) Total bacteria load assessment of *E. coli* in urine using the WST-8–mPMS metabolic module integrated in the plastic container. (B) Species-specific identification of *E. coli* in urine using the HRP-antibody/TMB immunoassay module integrated in the same device. (C) Representative photograph of the integrated plastic-container device used for parallel dual-mode detection from a single urine sample. Data are presented as mean ± SD (n = 5), with CV values shown. Statistical significance is indicated as $p < 0.01$ (**), and $p < 0.001$ (***).

quantification of bacteria load, showing reliable performance for both *E. coli* and *S. aureus* across concentrations ranging from 5×10^4 to 10^8 CFU mL^{-1} in different sample matrices. In the integrated device, the two modules provided parallel readouts from a single urine sample using spatially separated detection spots within one plastic container. These findings validate the robustness and versatility of the VFA architecture, demonstrating its adaptability for metabolic or immunological detection and its integration potential for multiplex POCT.

Discussion

This study establishes a single-sample, dual-mode VFA that integrates species-specific immunodetection and total viable bacteria-load assessment within one paper-based device. The developed dual-mode VFA combines an HRP-antibody/TMB immunoassay with a WST-8–mPMS metabolic module, enabling complementary information on bacteria identity and overall burden to be obtained from a single urine sample. Importantly, the two readouts are generated from spatially separated detection spots within the same integrated device rather than from a single shared test zone, allowing parallel operation while minimizing chemical and optical interference between the two colorimetric reactions. Given that *E. coli* is the leading causative agent of UTIs, accounting for approximately 75–85% of uncomplicated UTI cases, it was selected as the primary target for evaluating species-specific identification in this study.[18,19] Across TSB and urine matrices, the platform produced visually distinguishable and quantitatively interpretable responses, with statistically significant discrimination around the clinically relevant threshold of 10^5 CFU mL^{-1}.[22–24] The detection range was defined from 5×10^4 to 10^8 CFU mL^{-1}, and 10^5 CFU mL^{-1} was used as a clinically relevant bacteriuria decision threshold for assay evaluation rather than as a formally calculated LOD. Rather than emphasizing maximum analytical sensitivity, this study highlights a clinically aligned sensing strategy for rapid POCT assessment of both pathogen identity and decision-level bacteria load.

Selection of PT-R7 as the detection layer

According to the red ink flow test results, initial trials using the Whatman 1454-185 paper (Experimental ID ③) produced uniformly intense color signals across all *E. coli* concentrations (Table S7). However, the absence of a concentration-dependent gradient indicated excessive background and limited quantitative resolution. To overcome this limitation, the Whatman substrate was replaced with PT-R7, a conjugate-release matrix commonly employed in LFA.[24,31,32] When incorporated into the vertical-flow configuration, PT-R7 markedly improved signal discrimination among bacteria concentrations (Fig. S1), yielding a clear positive correlation fitted by both Hill and linear models (R^2 = 0.7051 and 0.6136, respectively). This improvement can be attributed to the material's more uniform liquid transport and reduced reagent over-retention, which together lowered background coloration and improved sensitivity. PT-R7 was selected as the detection layer because its interwoven cellulose-glass-fiber mesh provides a high surface area and strong capillary action.[24,28,30,31,34] In contrast to conventional nitrocellulose membranes, which exhibit rapid wicking and strong but often irreversible protein adsorption that can limit controlled reagent release and residence time in enzyme-based assays, PT-R7 enables more controlled fluid transport and reagent retention. The conjugate-release matrix structure supports high loading of antibodies, enzyme labels, and gold nanoparticles, while enabling uniform rehydration and stable signal development.[28–30,33,36] The surface chemistry of PT-R7 enables passive adsorption through electrostatic, hydrogen-bonding, and hydrophobic interactions, eliminating the need for chemical coupling and simplifying fabrication while preserving biological activity.[24,29,30,32,34] Upon rehydration, PT-R7 facilitates controlled release of pre-deposited reagents rather than permanent sequestration, resulting in consistent signal generation and reduced variability.[30] In addition to its analytical advantages, PT-R7 offers excellent process compatibility. It endures dry storage, retains mechanical integrity during lamination, and readily accommodates hydrophilic channel patterning.[28–30] These features mirror its established role in LFAs as a conjugate or release pad, where on-demand reagent delivery after rehydration is essential.[24,28–33] Overall, the optimized capillary flow, enhanced protein adsorption, and manufacturing robustness of PT-R7 significantly improved signal clarity and reproducibility in the vertical-flow format.[30] These characteristics confirm PT-R7 as a high-performance detection substrate that enhances both analytical performance and device manufacturability.

Vertical flow architecture and fluid control

The core design centers on the vertical flow immunoassay device. A PT-R7 detection layer was coupled to a five-layer absorbent stack arranged from top to bottom as one sheet of Whatman 1454 (pore size 22 μm, Experimental ID ③), two sheets of Whatman 1003 (pore size 6 μm, Experimental ID ⑥), and two sheets of high-absorbency blotting paper (Fig. 1C). This graded-pore structure regulated capillary flow and mass transport (Fig. 1A and C). As liquid moved from larger to smaller pores, flow velocity decreased and residence time at the detection interface increased, enhancing antigen–antibody binding and enzymatic turnover. Unlike conventional microfluidic devices that rely on rigid hydrophobic barriers to strictly confine lateral flow, the presented vertical flow architecture prioritized capillary-driven vertical transport within a porous matrix. Consequently, limited lateral diffusion within the detection layer is expected in this architecture. This design trade-off favors robustness, ease of fabrication, and tolerance to user handling, which are critical considerations for POCT applications.

The graded structure also selectively retains bound immunocomplexes within the upper layers while allowing unbound antibodies and small molecules to percolate downward, thereby reducing background and stabilizing the baseline. These features concentrate analytes at the reaction interface and promote uniform penetration across the detection zone, yielding reproducible transport and improved signal clarity. The washing step remains necessary for the HRP-antibody/TMB immunodetection module because it removes unbound HRP-conjugated antibodies and residual urinary matrix components, thereby reducing nonspecific background signals. Although washing steps increase operational complexity and may introduce user-dependent variation in POCT use, this issue was partially mitigated in the current prototype by incorporating guided flow channels into the sample injection plate. These channels direct both the sample and washing buffer into the predefined detection spots in a stable and controlled manner (Fig. 1B and C). This design reduces the need for users to manually target each reaction zone and helps lower dispensing-related errors. Nevertheless, further simplification of the washing process, such as preloaded washing buffer or absorbent-layer-controlled automatic washing, will be important for future product-oriented development.

SEM verification of bacterial transport in the WST-8–mPMS module

For the WST-8–mPMS metabolic readout, a simplified two-layer format was used. The top filter layer was Whatman 1454, which removed common matrix particulates such as cellular debris, exfoliated epithelial cells, mucus, colloidal protein aggregates, and amorphous urinary salts or crystals before the filtrate reached the detection layer, reducing fouling and variability while preserving rapid assay kinetics. To further verify bacteria transport through this two-layer configuration, SEM was performed after applying *S. aureus* (10^8 CFU mL^{-1}) onto the optimized stack. Control samples without bacteria showed only the fibrous microstructure of the filter and detection layers, whereas bacteria-treated samples revealed *S. aureus* adhering to the fiber surfaces of both layers (Fig. S2). These results confirm that bacteria can traverse the upper filtration layer and reach the underlying detection layer under capillary-driven flow. This observation supports the functional design of the WST-8–mPMS metabolic module, which relies on controlled bacteria permeation to enable total-load quantification. In contrast, the species-specific immunoassay confines antigen–antibody binding within the top PT-R7 layer, whose tighter pore structure and immobilized antibodies prevent cellular penetration, thereby preserving assay specificity.

Species-specific immunoassay performance

The HRP-antibody/TMB readout showed clear concentration-dependent responses for *E. coli* in both TSB and urine. In TSB, model fits indicated moderate quantitative behavior (Hill R^2 = 0.7422; linear R^2 = 0.7718) with a maximum CV of 20.15% at 10^6 CFU mL^{-1} (Fig. 3A, B and E). In urine, correlation improved (Hill R^2 = 0.8643; linear R^2 = 0.8764), and visual discrimination remained robust across 5 × 10^4 to 10^8 CFU mL^{-1}, supporting applicability to clinically relevant samples (Fig. 3C–E). Importantly, the intrinsic coloration of urine did not compromise assay performance, as background-referenced grayscale analysis effectively decoupled sample color from enzymatic signal intensity. This robustness is critical for POCT deployment, where sample appearance can vary substantially between individuals. Performance trends align with immunoassay architecture. The PT-R7 detection layer affords high surface area and uniform wicking, which supports dense antibody immobilization and homogeneous wetting of the reaction zone. The downstream pore gradient increases residence time at the interface and limits downward transport of unbound species, which reduces background and sharpens contrast (Fig. 1A).

The remaining signal variability is likely associated with non-uniform liquid distribution, spatially heterogeneous color development within the porous paper matrix, and reaction-zone geometry rather than the antibody–antigen reaction alone. Variability at high bacteria loads is attributable to transport limitations and interfacial crowding within the porous detection layer rather than to the antibody–antigen reaction. Such spatial heterogeneity is intrinsic to paper-based assays and underscores the importance of standardized image-based averaging rather than sampling for quantitative analysis. Rapid capillary advection can shorten residence time and create uneven infiltration, while dense fluxes of cells and immune complexes partially occlude pores and saturate local binding sites. These conditions promote rapid local substrate depletion, accumulation of colored products, and occasional spillover into adjacent zones, all of which amplify signal spread. Incremental improvements are expected from tighter control of dispensing volume and rate, modest enlargement or repositioning of reaction spots to balance lateral spreading with vertical flow, and small adjustments to wash stringency to stabilize the baseline. Overall, the species-specific immunoassay maintains quantifiable behavior in TSB and urine and provides visually discriminable readouts over a clinically meaningful range.

Quantitative total bacteria performance

The WST-8–mPMS metabolic readout enabled rapid quantification of total bacteria load and extended the platform beyond species specificity. Using the two-layer format for this assay, both *E. coli* and *S. aureus* were measured across 5 × 10^4 to 10^8 CFU mL^{-1} in TSB and urine, demonstrating cross-species and cross-matrix applicability. Linear models showed consistent concentration–signal relationships. For *E. coli*, R^2 = 0.84 in TSB and R^2 = 0.82 in

urine (Fig. 4A and B). For *S. aureus*, R^2 = 0.72 in TSB and R^2 = 0.78 in urine (Fig. 4C and D). The grayscale response decreased monotonically with increasing bacteria concentration, reflecting stronger color development at higher metabolic activity and enabling straightforward standard-curve calibration with smartphone imaging. These measurements confirmed that the WST-8–mPMS module can provide a species-independent metabolic readout of total viable bacteria load. Practical advantages include minimal sample preparation, compatibility with complex matrices, and stable operation with a front-end filtration layer that reduces particulates and fouling before the reagent layer. Although these module-level measurements were performed outside the final integrated cartridge, they provided the analytical basis for incorporating the WST-8–mPMS assay into the spatially separated metabolic detection spots of the integrated dual-mode device.

Integrated plastic container for species-specific and quantitative urine testing

By integrating the HRP-antibody/TMB immunoassay and WST-8–mPMS metabolic modules within one plastic-container-based vertical flow device, the cartridge delivered species-specific recognition and total-load assessment from a single urine sample. Each plastic container contained four spatially separated reaction sites: two configured for HRP-antibody/TMB immunodetection and two for WST-8–mPMS metabolic detection. This spatial separation allowed the two colorimetric reactions to proceed in parallel while minimizing chemical and optical interference.

When urine samples were tested, both the metabolic and species-specific channels showed concentration-dependent responses across the tested range. For the WST-8–mPMS metabolic module, statistically significant differences were observed between 5×10^4 and 10^7 CFU mL^{-1} and between 5×10^4 and 10^8 CFU mL^{-1} (Fig. 5A). For the HRP-antibody/TMB immunodetection module, a significant difference was observed between 5×10^4 and 10^8 CFU mL^{-1} (Fig. 5B). These results support threshold-oriented assessment across a concentration range spanning the clinically relevant bacteriuria level of 10^5 CFU mL^{-1}, rather than representing a formally calculated limit of detection.

Variability in the prototype arose mainly from fluid distribution, spatially heterogeneous color development, and spot geometry rather than from the sensing chemistries themselves. The highest CV, around 24.82%, occurred at 5×10^4 CFU mL^{-1}. More refined hydrophilic patterning, improved control of dispensing volume and rate, and minor adjustments to washing and absorbent stacking are expected to reduce signal spread while preserving simultaneous readouts. Overall, the integrated cartridge demonstrates that species identity and total bacteria load can be obtained in parallel within a compact, single-sample workflow, supporting multiplex POCT screening. Unlike conventional ELISA, which requires multiple manual handling steps, trained personnel, and benchtop instrumentation, the presented VFA emphasizes operational simplicity, smartphone-based readout, and early result visibility, making it more suitable for decentralized and resource-limited settings.

Limitations and comparison to existing methods

This study establishes a modular dual-mode vertical flow architecture, while further refinement of fluid distribution and reaction-zone geometry should improve linearity and precision across the full concentration range. Variability observed in some configurations arose chiefly from non-uniform liquid distribution, spatially heterogeneous color development within the porous paper matrix, and reaction-zone geometry, rather than from the underlying immunochemical or metabolic reactions alone. Urine also introduced matrix effects that may compress the dynamic range. These limitations are tractable engineering targets: more uniform sample delivery, refined hydrophilic patterning, modest adjustments to wash conditions, and matrix-matched calibration can all reduce spread and stabilize the baseline.

Several limitations should also be noted. First, the washing step remains necessary for the HRP-antibody/TMB immunodetection module to remove unbound HRP-conjugated antibodies and reduce nonspecific background. Although the sample injection plate with guided flow channels reduces direct manual targeting of the reaction zones, washing still adds operational complexity and may introduce user-dependent variation. Second, the present study used *S. aureus* as a Gram-positive non-target control for initial specificity evaluation; therefore, the current data should be interpreted as proof-of-concept *E. coli*-specific detection rather than comprehensive specificity validation across a full uropathogen panel. Broader pathogen-panel testing would be required before practical diagnostic translation. Third, 10^5 CFU mL^{-1} was used as a clinically relevant decision threshold for assay evaluation, and a formal LOD was not determined in this pilot study. To better position the proposed sensing strategy within the context of existing bacteria detection approaches, a comparison of representative methods is summarized in Table 1.

Conventional bacteria detection techniques differ in their ability to provide species identification, bacteria load estimation, analysis time, and instrumentation requirements. While culture-based assays can provide both identification and quantification, they typically require long incubation times (24–72 h). Molecular techniques such as PCR offer rapid species identification but generally do not directly quantify total bacteria load. Compared with plate ELISA methodology, the described platform reduces steps, time, and instrument dependence while preserving species specificity.[1,2,11,15,20,21] In contrast, metabolic assays estimate overall bacteria activity but lack species specificity. These limitations highlight the need for diagnostic platforms

Table 1 Comparison of representative bacteria detection methods and the proposed dual-mode VFA

Method	Species identification	Total bacteria quantification	Detection time	Instrument
Culture	V	V	24–72 h	Incubator
PCR	V	×	1–3 h	Thermocycler
Immunoassay	V	Limited	2–4 h	Reader
Metabolic assay	×	V	1–2 h	Reader
This work (dual-mode VFA)	V	V	35–40 min	Smartphone

capable of simultaneously reporting both bacteria identity and bacteria load within a rapid and simple workflow.

In practical use, pre-fabricated and reagent-preloaded VFA cartridges could be taken directly from storage and used for testing, without on-site fabrication or assay preparation. Under this use scenario, both species-specific immunoassay and total bacteria load readouts are obtained within approximately 35–40 min from a single urine sample, enabling simultaneous identification and quantification in one test. Compared with culture plate methodology, this approach offers rapid readouts relevant for triage, albeit without the definitive organism growth information that culture provides. Relative to qPCR, this approach trades ultimate sensitivity and genotypic detail for simpler workflows and lower cost.[20] Compared with conventional LFAs, the vertical architecture enables controlled residence time, analyte retention, and multiplexable layouts. Despite modest R^2 values in select cases, the present results support threshold-oriented bacteria screening across a clinically relevant concentration range rather than definitive diagnostic confirmation.

Despite the widespread use of HRP-antibody/TMB colorimetric immunoassays in LFAs and VFAs, most reported systems are designed as single-mode assays that provide only species-specific binding readouts.[3,10,14–16,31,32] In these platforms, performance improvements are typically pursued through antibody optimization, multilayer delays, or signal amplification strategies. In contrast, the present work does not aim to introduce a new HRP–TMB chemistry or a new WST-8–mPMS reaction. Instead, it integrates these established chemistries into a dual-mode vertical flow platform that simultaneously reports species identity and total bacteria load through spatially separated detection spots within one device. This system-level integration enables contextual interpretation at clinically relevant thresholds, which is not addressed by conventional single-mode HRP–TMB-based LFA or VFA.

Conclusions

In this study, we developed a dual-mode VFA that integrated species-specific immunodetection and quantitative total bacteria assessment within one integrated paper-based vertical flow device. By combining an HRP-antibody/TMB immunoassay with a WST-8–mPMS metabolic readout, the system enabled complementary immunological and metabolic information to be obtained from a single urine sample through spatially separated detection spots. The platform demonstrated threshold-oriented detection across 5×10^4 to 10^8 CFU mL^{-1}, spanning the clinically relevant bacteriuria decision level of 10^5 CFU mL^{-1}, in both TSB and human urine, supported by smartphone-based grayscale analysis without dedicated instrumentation. Initial species-specific detection of *E. coli* was demonstrated with minimal cross-reactivity against the tested Gram-positive non-target bacterium, *S. aureus*, while the metabolic module enabled species-agnostic quantification of total viable bacteria load across multiple matrices. These results support the feasibility of using the platform to simultaneously report target bacterial identity and total bacteria load within a single integrated test. The findings establish a practical framework for POCT bacteria screening and triage, where rapid assessment at clinically actionable thresholds can guide downstream confirmatory testing. While further engineering refinements and broader pathogen-panel validation may improve precision and scalability, the present work demonstrates that dual-mode bacteria detection can be achieved with minimal assay complexity, supporting decentralized and resource-limited diagnostic settings.

Institutional review board

Approval was obtained from the Institutional Review Board of National Cheng Kung University Hospital in Taiwan (NCKU IRB No. B-BR-109-056). Informed consent was obtained from the subjects involved in the study.

Author contributions

Shu-Yun Sheu: writing – review & editing, writing – original draft, methodology. Ching-Fen Shen: writing – review & editing, writing – original draft, conceptualization, supervision, methodology. Chao-Min Cheng: writing – review & editing, writing – original draft, supervision, conceptualization.

Conflicts of interest

The authors have no interests to declare.

Abbreviations

BSA	Bovine serum albumin
CFU	Colony-forming unit
CV	Coefficient of variation

E. coli	*Escherichia coli*
EDTA	Ethylenediaminetetraacetic acid
ELISA	Enzyme-linked immunosorbent assay
HRP	Horseradish peroxidase
LFA	Lateral flow assay
LOD	Limit of detection
LPS	Lipopolysaccharide
mPMS	1-Methoxy phenazine methosulfate
PBS	Phosphate-buffered saline
PCR	Polymerase chain reaction
POCT	Point-of-care testing
RGB	Red, green, and blue channel
ROI	Region of interest
S. aureus	*Staphylococcus aureus*
SEM	Scanning electron microscope
TMB	3,3′,5,5′-Tetramethylbenzidine
TSB	Tryptic soy broth
UTI	Urinary tract infection
VFA	Vertical flow assay
WST-8	Water-soluble tetrazolium salt-8

Data availability

The data and materials for this study are available from the corresponding authors upon reasonable request.

Supplementary information (SI) is available. See DOI: https://doi.org/10.1039/d6lc00265j.

Acknowledgements

This research was funded by Taiwan's National Science and Technology Council (113-2221-E-007-021-MY3, 114-2622-B-006-007 & 113-2622-E-007-019).

References

1 S.-Y. Sheu, C.-M. Cheng and C.-F. Shen, Current status and future perspectives of vertical flow assays, *Trends Biotechnol.*, 2026, **44**, 40–52.
2 N. Jiang, R. Ahmed, M. Damayantharan, B. Ünal, H. Butt and A. K. Yetisen, Lateral and Vertical Flow Assays for Point-of-Care Diagnostics, *Adv. Healthcare Mater.*, 2019, **8**(14), 1900244.
3 P. Chen, M. Gates-Hollingsworth, S. Pandit, A. Park, D. Montgomery, D. AuCoin, J. Gu and F. Zenhausern, based Vertical Flow Immunoassay (VFI) for detection of bio-threat pathogens, *Talanta*, 2019, **191**, 81–88.
4 B. Liu, Q. Liu, K. Zhong, W. Wu, S. Zheng, W. Yao, B. Gao and F. Sun, Enhanced SERS-based vertical flow assay for high sensitivity multiplex analysis of antibiotics, *Microchem. J.*, 2024, **199**, 110008.
5 M. Moumita, K. Shankar, P. Abhiman and B. Shamasundar, Development of a sandwich vertical flow immunogold assay for rapid detection of oxytetracycline residue in fish tissues, *Food Chem.*, 2019, **270**, 585–592.
6 S. Kim, Y. Hao, E. A. Miller, D. M. Tay, E. Yee, P. Kongsuphol, H. Jia, M. McBee, P. R. Preiser and H. D. Sikes, Vertical flow cellulose-based assays for SARS-CoV-2 antibody detection in human serum, *ACS Sens.*, 2021, **6**(5), 1891–1898.
7 R. Lei, D. Wang, H. Arain and C. Mohan, Design of gold nanoparticle vertical flow assays for point-of-care testing, *Diagnostics*, 2022, **12**(5), 1107.
8 H.-A. Joung, Z. S. Ballard, A. Ma, D. K. Tseng, H. Teshome, S. Burakowski, O. B. Garner, D. Di Carlo and A. Ozcan, based multiplexed vertical flow assay for point-of-care testing, *Lab Chip*, 2019, **19**(6), 1027–1034.
9 J. L. Vaitukaitis, G. D. Braunstein and G. T. Ross, A radioimmunoassay which specifically measures human chorionic gonadotropin in the presence of human luteinizing hormone, *Am. J. Obstet. Gynecol.*, 1972, **113**(6), 751–758.
10 J. Park and J.-K. Park, Pressed region integrated 3D paper-based microfluidic device that enables vertical flow multistep assays for the detection of C-reactive protein based on programmed reagent loading, *Sens. Actuators, B*, 2017, **246**, 1049–1055.
11 R. Lei, H. Arain, M. Obaid, N. Sabhnani and C. Mohan, Ultra-sensitive and semi-quantitative vertical flow assay for the rapid detection of interleukin-6 in inflammatory diseases, *Biosensors*, 2022, **12**(9), 756.
12 J. Wang, K. Mu, H. Wei, H. Chen, Y. Wang, W. Zhang and Z. Rong, based multiplex colorimetric vertical flow assay with smartphone readout for point-of-care detection of acute kidney injury biomarkers, *Sens. Actuators, B*, 2023, **390**, 134029.
13 O. Clarke, B. Goodall, H. Hui, N. Vats and C. Brosseau, Development of a SERS-based rapid vertical flow assay for point-of-care diagnostics, *Anal. Chem.*, 2017, **89**(3), 1405–1410.
14 D. M. Tay, S. Kim, Y. Hao, E. H. Yee, H. Jia, S. M. Vleck, M. Chilekwa, J. Voldman and H. D. Sikes, Accelerating the optimization of vertical flow assay performance guided by a rational systematic model-based approach, *Biosens. Bioelectron.*, 2023, **222**, 114977.
15 A. Goncharov, H. A. Joung, R. Ghosh, G. R. Han, Z. S. Ballard, Q. Maloney, A. Bell, C. T. Z. Aung, O. B. Garner and D. D. Carlo, Deep Learning-Enabled Multiplexed Point-of-Care Sensor using a Paper-Based Fluorescence Vertical Flow Assay, *Small*, 2023, **19**(51), 2300617.
16 M. Kaur and E. Eltzov, Optimizing effective parameters to enhance the sensitivity of vertical flow assay for detection of Escherichia coli, *Biosensors*, 2022, **12**(2), 63.
17 Z. Gu, H. Chang, G. Yang, B. Xu, B. Miao and J. Li, An integrated electronic tag-based vertical flow assay (e-VFA) with micro-sieve and AlGaN/GaN HEMT sensors for multi-target detection in actual saliva, *Analyst*, 2024, **149**(16), 4267–4275.
18 M. T. Nüesch-Inderbinen, M. Baschera, K. Zurfluh, H. Hächler, H. Nüesch and R. Stephan, Clonal diversity, virulence potential and antimicrobial resistance of Escherichia coli causing community acquired urinary tract infection in Switzerland, *Front. Microbiol.*, 2017, **8**, 2334.
19 B. Foxman, The epidemiology of urinary tract infection, *Nat. Rev. Urol.*, 2010, **7**(12), 653–660.

20 M. Tahmasebi, T. Bamdad, W. E. Svendsen and M. Forouzandeh-Moghadam, An enzymatic nucleic acid vertical flow assay, *Anal. Bioanal. Chem.*, 2022, **414**(12), 3605–3615.
21 R. Chen, X. Du, Y. Cui, X. Zhang, Q. Ge, J. Dong and X. Zhao, Vertical flow assay for inflammatory biomarkers based on nanofluidic channel array and SERS nanotags, *Small*, 2020, **16**(32), 2002801.
22 E. H. Kass, Asymptomatic infections of the urinary tract, *J. Urol.*, 2002, **167**(2), 1016–1020.
23 M. L. Wilson and L. Gaido, Laboratory diagnosis of urinary tract infections in adult patients, *Clinical infectious diseases*, 2004, **38**(8), 1150–1158.
24 G. Schmiemann, E. Kniehl, K. Gebhardt, M. M. Matejczyk and E. Hummers-Pradier, The diagnosis of urinary tract infection: a systematic review, *Dtsch. Arztebl. Int.*, 2010, **107**(21), 361.
25 M. Serhan, D. Jackemeyer, K. Abi Karam, K. Chakravadhanula, M. Sprowls, P. Cay-Durgun and E. Forzani, A novel vertical flow assay for point of care measurement of iron from whole blood, *Analyst*, 2021, **146**(5), 1633–1641.
26 J. Li and J. Macdonald, Multiplexed lateral flow biosensors: Technological advances for radically improving point-of-care diagnoses, *Biosens. Bioelectron.*, 2016, **83**, 177–192.
27 R. Chen, J. Wu, H. Wang, M. S. Nisar, Y. Li, Y. Chen, Y. Mao, X. Nan, F. Zhang and L. Yang, Fe3O4@ Au magnetic SERS nanotags-based vertical flow immunoassay for simultaneous detection of fumonisin B1, aflatoxin B1 and deoxnivalenol, *Anal. Chim. Acta*, 2025, **1348**, 343837.
28 V. Borse and R. Srivastava, Process parameter optimization for lateral flow immunosensing, *Mater. Sci. Energy Technol.*, 2019, **2**(3), 434–441.
29 M. Sajid, A.-N. Kawde and M. Daud, Designs, formats and applications of lateral flow assay: A literature review, *J. Saudi Chem. Soc.*, 2015, **19**(6), 689–705.
30 N. Abu, N. Mohd Bakhori and R. H. Shueb, Lateral flow assay for hepatitis B detection: a review of current and new assays, *Micromachines*, 2023, **14**(6), 1239.
31 K. M. Koczula and A. Gallotta, Lateral flow assays, *Essays Biochem.*, 2016, **60**(1), 111–120.
32 B. O'Farrell, Lateral Flow Technology for Field-Based Applications—Basics and Advanced Developments, *Top. Companion Anim. Med.*, 2015, **30**, 139–147.
33 N. Alam, L. Tong, Z. He, R. Tang, L. Ahsan and Y. Ni, Improving the sensitivity of cellulose fiber-based lateral flow assay by incorporating a water-dissolvable polyvinyl alcohol dam, *Cellulose*, 2021, **28**(13), 8641–8651.
34 T. Tezcan, M. Calimci, I. H. Boyaci and U. Tamer, UV-ozone treated glass fiber based lateral flow DNA extraction platform integrated with LAMP for rapid detection of pathogen bacteria in whole blood, *Microchem. J.*, 2024, **206**, 111487.
35 C.-H. Chen, Y.-H. Liao, M. Muljadi, T.-T. Lu and C.-M. Cheng, Potential Application of the WST-8-mPMS Assay for Rapid Viable Microorganism Detection, *Pathogens*, 2023, **12**(2), 343.
36 C. Parolo, A. Sena-Torralba, J. F. Bergua, E. Calucho, C. Fuentes-Chust, L. Hu, L. Rivas, R. Álvarez-Diduk, E. P. Nguyen and S. Cinti, Tutorial: design and fabrication of nanoparticle-based lateral-flow immunoassays, *Nat. Protoc.*, 2020, **15**(12), 3788–3816.

